*Sensors and Materials*, Vol. 29, No. 12 (2017) 1749–1761
MYU Tokyo



S & M 1467

# Softening Hard Stool Using Magnetically Controlled $Fe_3O_4$ Nanoparticles

Qian Li, Xiaojun Liu, Ming Chang,[1,2*] Wei Hsiu Lin,[2] and Zhen Lu[3]

State Key Laboratory of Digital Manufacturing Equipment and Technology,
Huazhong University of Science and Technology, Wuhan 430074, China
[1]College of Mechanical Engineering and Automation, Huaqiao University, Xiamen 361021, Fujian, China
[2]Department of Mechanical Engineering, Chung Yuan Christian University, Chung Li 32023, Taiwan
[3]School of Economics and Management, Shanghai University of Electric Power, Shanghai 201300, China

(Received May 2, 2017; accepted December 5, 2017)

***Keywords:*** fecal impaction, oscillating magnetic field, $Fe_3O_4$ nanoparticle aggregate, hard stool, sway motion

Fecal impaction is a gastrointestinal problem that occurs in all age groups. Traditional therapy with drugs or surgery may result in serious complications for patients. Softening hard stool *in vitro* is realized with swaying $Fe_3O_4$ nanoparticle (NP) aggregates controlled by an oscillating magnetic field generated using a combination of electromagnetic coils and permanent magnets. The operation mechanism of the combined oscillating magnetic field is analyzed, experiments on NP manipulation by the magnetic field are conducted, and the morphology and sway motion characteristics of the aggregates are observed under various experimental parameter settings. Experimental results show that such NP aggregates manipulated by oscillating magnetic fields can be applied to soften stool in the rectum for fecal impaction treatment. In addition, diagnosis and sensing of constipation induced by obstruction in the gastrointestinal tract can be executed by the same approach in the future.

## 1. Introduction

Fecal impaction, a symptom of constipation in the presence of hard stool obstructing the rectum, is a common serious medical condition for a considerable number of people, with a higher prevalence in children, incapacitated patients, and the elderly.[1,2] Complications attributable to fecal impaction include stercoral ulceration, rectovaginal fistula, megacolon, and colonic perforation, which are associated with high morbidity and high mortality.[3] Traditional therapies include hard stool fragmentation or manual disimpaction, and hard stool softening using enemas followed by distal colon for evacuation.[1,2,4] The iatrogenic injury of the sphincter muscles leading to megarectum is occasionally found after manual disimpaction, and bowel necrosis, perforation, and death are occasionally encountered after cleansing using soap-sud enemas.[5,6] Surgery is reserved for peritonitis induced by bowel perforation. However, patients are required to tolerate pain and there is a risk of complication.[7] Moreover, clinical sensing of such sickness is usually based on reduced defecation frequency or difficulty in defecation, which, however, always indicate

*Corresponding author: e-mail: ming@cycu.edu.tw
http://dx.doi.org/10.18494/SAM.2017.1817

that the patients are in a serious condition. Early diagnosis and a fast and painless treatment for fecal impaction are thus desirable.

Magnetic nanomaterials have been applied in various biomedical applications, such as in cell marking and separation, targeted drug delivery, thermotherapy, and magnetic resonance contrast enhancement, and have been found to be biocompatible and suitable for pain-free microsurgery.[8–10] The noncontact motion control of magnetic nanomaterials has been investigated. Fan *et al.*[11] observed the rotation of gold, platinum, and nickel nanowires in an alternating electric field. Wang *et al.*[12] controlled the rotation and translation of microrods using ultrasonic waves. Rikken *et al.*[13] reviewed the manipulation of micro- and nanostructure motion using magnetic fields, including homogeneous and inhomogeneous magnetic fields, and rotating and oscillating magnetic fields. These investigations showed that the motion of magnetic materials can be controlled by various noncontact methods. Shaalan *et al.*[10] reported that the major trend in nanomaterials is to make them multifunctional and controllable using external signals or in accordance with the local environment. Many biological and biomedical experiments that utilize these motions have been carried out, with encouraging results. Zhang *et al.*[14] controlled the motion of blood cells with rotational nickel nanowires. Zhou and Metin[15] proposed an approach for the fluidic trapping and two-dimensional transport of swimming microorganisms, which utilizes a rotating magnetic microrobot. Gabayno *et al.*[16,17] developed thrombolysis technology, in which a strong vortex is induced by rotating magnetic aggregates for breaking a thrombus. These experiments indicate that micro- and nanomaterials can impact the target indirectly with the help of a rotational fluid induced by fast rotating micro- or nanomaterials. Simultaneously, controlling a microrobot to move with a magnetic field and a field gradient has been reported in many studies. Chanu and Martel[18] proposed a magnetic resonance imaging (MRI)-system-based method for driving microrods. Yesin *et al.*[19] and Choi *et al.*[20] actuated a ferromagnetic microrobot with Helmholtz and Maxwell coil pairs.

Similar to previous biological experiments on the manipulation of micro- and nanostructures, we propose a swaying nanoparticle (NP) aggregate approach to break and soften hard stools by contact. Experiments are carried out in a microfluidic channel. $Fe_3O_4$ NPs are first magnetized to form aggregates by a static magnetic field generated by two permanent magnets and then these aggregates are controlled to sway around their centroid by a perpendicular oscillating magnetic field produced by two electromagnetic coils driven by an alternating current. The magnetic force guides the aggregate forward onto the target to break the stool block and sweep the pieces away. Experiments show that various sizes of the aggregates formed by the magnetic field can be used to perform the breaking action. Because of the good characteristics of the contrast agent of $Fe_3O_4$ NPs, it is also possible to incorporate the proposed approach with MRI or other bioimaging technologies to achieve the target of early detection of fecal impaction by magnetically controlling the movement of the magnetic nanomaterials.

## 2. Materials and Methods

### 2.1 Preparation of $Fe_3O_4$ NPs

$Fe_3O_4$ NPs were prepared by the coprecipitation method. 100 ml of a 0.1 M $FeCl_2$ solution and 100 ml of a 0.2 M $FeCl_3$ solution were mixed in a 500 ml beaker and stirred with a glass rod. 100 ml of a 0.8 M NaOH solution was continuously added and then the mixture was stirred vigorously

for about 30 min. Finally, a strong permanent magnet was used to attract the black precipitates to the bottom and then the supernatant was removed. Deionized water was added to purify the precipitates five to six times to ensure a pH of about 7.0. The precipitates were then dried and ground to obtain $Fe_3O_4$ particles. After the particles were dispersed in deionized water again, they were broken into nanometer scale with an ultrasonic processor.

## 2.2 Experimental methods

### 2.2.1 Experimental setup

A schematic diagram of the experimental setup is shown in Fig. 1. Two permanent magnets are placed to generate a static unidirectional magnetic field $H_s$. Magnetic NPs in the microfluidic capillary magnetized by the unidirectional field tend to aggregate owing to the action of dipolar attractive forces. A pair of electromagnetic coils, into which an alternating current from a programmable source (not shown) is input, are placed orthogonally to the static field and generate a sinusoidal dynamical field $H_v$ with an amplitude of $H_p$ and a frequency of $f$, i.e., $H_v = H_p\sin(2\pi ft)$. Under such a magnetic field configuration, the combined oscillating magnetic field is $\vec{H} = H_s\vec{i} + H_v\vec{j}$, in which $\vec{i}$ and $\vec{j}$ are unit vectors in the $x$- and $y$-axes. The phase angle trajectory (denoted as $\varphi$) of the combined oscillating field is

$$\varphi = \tan^{-1}\left[\frac{H_p \sin(2\pi ft)}{H_s}\right]. \tag{1}$$

The magnetic NP aggregates tend to align their easy axis along the orientation of the final magnetic field and will oscillate (denoted as a sway motion) under this combined oscillating magnetic field. A high-speed camera is used to observe the experimental process in a microfluidic capillary surrounded by magnets and coils.

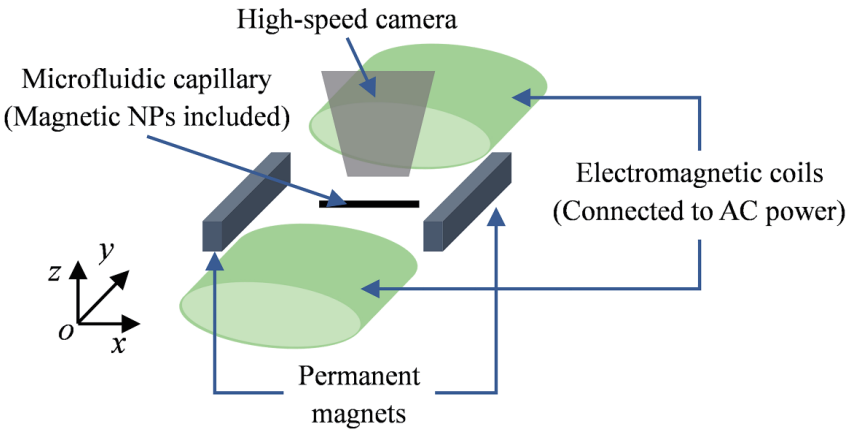


Fig. 1. (Color online) Schematic diagram of experimental setup consisting of two permanent magnets, two electromagnetic coils into which AC current is applied, a high-speed camera, and microfluidic capillary.

### 2.2.2 Principle of softening stool

The mechanism of softening stool is the sway motion of $Fe_3O_4$ NP aggregates. Under the action of a combination of a fluid field and a magnetic field, the forces applied to magnetic aggregates include contributions from drag force, magnetism, buoyancy force, gravitational force, Brownian force, thermophoretic force, Saffman's lift force, and Basset force.[21] Since only forces in the horizontal plane should be considered, buoyancy force and gravitational force in the vertical direction are neglected. Brownian force can be negligible since Brownian motion is not obvious for these aggregates. As there is almost no temperature difference in the capillary, the thermophoretic force is not taken into consideration. Saffman's lift force and Basset force are also neglected because they are generally much less than the drag force.[21]

The force and torque exerted on a $Fe_3O_4$ aggregate, which is simplified as an ellipsoid with a half-major axis of $a$ and a minor axis of $b$, are shown in Fig. 2. $\tau_m$ and $\tau_D$ are, respectively, the magnetic torque and drag torque. $\theta$ is the angle between the combined magnetic field $H$ and the easy axis (dashed line in the figure). $F_{mx}$ and $F_{my}$ are the components of magnetic force in the $x$- and $y$-axes, respectively. $F_D$ is the fluidic resistance when assuming that the aggregate moves in the $x$ direction. $F_x$ and $F_y$ are the interaction forces between the aggregate and the stool. Figure 2(b) shows the force acting on the stool from the aggregate.

The total drag torque exerted by the fluid on the ellipsoid aggregate rotating along the minor axis is[22]

$$\tau_D = 8\pi\omega k a^3 (s_0^2 + 1)^{3/2}, \tag{2}$$

where $s_0$ is a parameter that can be obtained in Ref. 22, $k = \frac{2}{3}\left(2s_0^2 + 1\right)\left[(1 - s_0)^2 \tan^{-1}\left(\frac{1}{s_0}\right) + s_0\right]^{-1}$, and $\omega$ is the rotational speed of the ellipsoid.

For a magnetic aggregate placed in a magnetic field $H$, the driving magnetic torque is[16]

$$\tau_m = \mu_0 \frac{\chi^2}{2(2+\chi)} V H^2 \sin(2\theta), \tag{3}$$

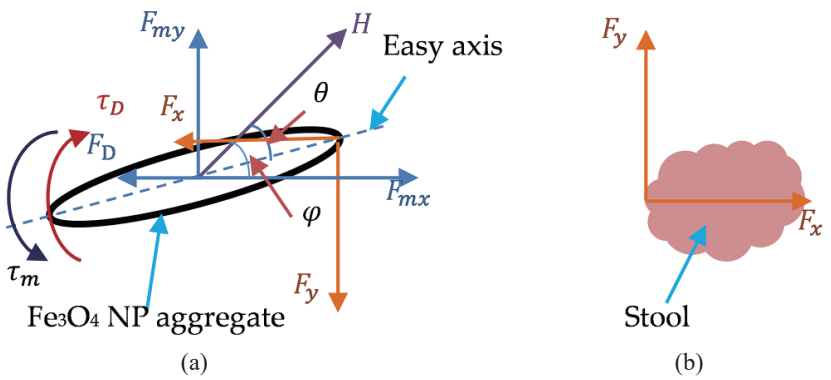


Fig. 2. (Color online) (a) Free-body diagram of swaying $Fe_3O_4$ aggregate when breaking stool. (b) Force acting on the stool from the aggregate.

where $V = 4\pi ab^2/3$ is the volume of the magnetic aggregate and $\chi$ is magnetic susceptibility.

Supposing that the aggregate rotates at a constant speed, $\tau_m$ is equal to $\tau_D$ at low Reynolds numbers and then the rotational speed can be obtained as[23]

$$\omega = \frac{\mu_0 \chi^2 V H^2 \sin(2\theta)}{16\pi k a^3 (2+\chi)(s_0^2+1)^{3/2}}. \tag{4}$$

When the aggregate moves at velocity $v$, the fluidic drag force applied to the aggregate is $F_D = 6\pi\eta r v$,[24] where $\eta$ is the viscosity coefficient and $r$ is the equivalent radius of the aggregate. However, when the aggregate presses against the stool, the motion of the aggregate is blocked by the stool, i.e., $F_D$ can be seen as zero. Therefore,[25,26]

$$\begin{cases} F_x = F_{mx} = \dfrac{3\chi}{3+\chi}\mu_0 V H \dfrac{\partial H}{\partial x}, \\ F_y = F_{my} = \dfrac{3\chi}{3+\chi}\mu_0 V H \dfrac{\partial H}{\partial y}, \end{cases} \tag{5}$$

where $\dfrac{\partial H}{\partial x}$ and $\dfrac{\partial H}{\partial y}$ are, respectively, the magnetic gradients in the $x$ and $y$ directions.

Equations (4) and (5) constitute the force model for the breaking of stool by a swaying aggregate. Six dry and hard stool blocks were prepared to check the strength of the stool. Experiments were carried out with the universal material testing machine WDW3200. Experimental results show that the tensile strength of these dry blocks is 0.02 ± 0.001 MPa. More conservatively, we may assume the contact force component $F_x$ to be an axial force applied to the stool and neglect $F_y$. Under the conditions of $H = 22$ Oe and $\dfrac{\partial H}{\partial x} = 0.2$ T/m, the induced $F_x$ is approximately $2 \times 10^{-8}$ N. In the case of a stool block with a cross-sectional area of $1 \times 10^{-12}$ m$^2$, the resulting maximum normal stress and shear stress applied to the stool are 0.02 and 0.01 MPa, respectively. Since stool in solution is composed of loose and softer structures, the resulting stresses caused by impact can break these structures. Certainly, the aggregates formed of NPs will be employed to provide a combined breaking force in the process. The interaction forces between the aggregate and bulk stool are not only to break the stool but also to push the aggregate to another target. Sometimes the aggregate will also be damaged by the collision. However, the NPs will aggregate again owing to the action of the magnetic field. Moreover, the direction of motion of the NP aggregate can be controlled by changing the direction of the magnetic gradient.

## 3. Results

### 3.1 Characterization of $Fe_3O_4$ NPs

The morphology and magnetic characteristics of the obtained $Fe_3O_4$ NPs are shown in Fig. 3. Figure 3(a) shows a transmission electron microscopy (TEM) image of the $Fe_3O_4$ NPs. The diameters of these spherical particles are about 10–20 nm. The size distribution of the NPs measured with a dynamic light-scattering particle size distribution analyzer (Horiba LB-550) is shown in Fig. 3(b). The iron oxide concentration of the tested dispersions is 0.5%. The vibrating sample magnetometer (VSM) data shown in Fig. 3(c) indicate that there is almost no hysteresis

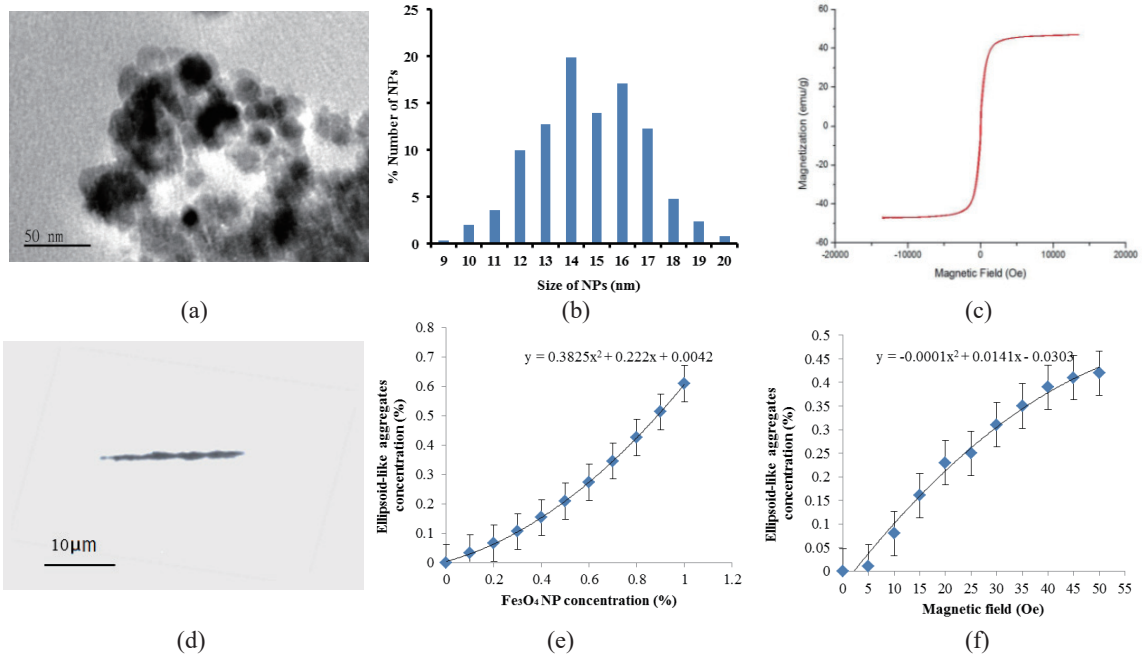


Fig. 3. (Color online) (a) TEM image of NPs, which are spherical in shape and have diameters of about 10–20 nm. (b) Size distribution of the NPs measured by dynamic light scattering. (c) Magnetic hysteresis loops from VSM measurements showing good magnetic characteristics. (d) SEM image of ellipsoid-like aggregate formed after permanent magnets were placed close to $Fe_3O_4$ suspension. (e) Relationship between ellipsoid-like aggregate concentration and $Fe_3O_4$ NP concentration under a magnetic field of 25 Oe. (f) Relationship between ellipsoid-like aggregate concentration and external magnetic field at the NP concentration of 0.5%.

when the magnetic field ranges from −15000 to 15000 Oe. This result confirms the good magnetic characteristics of the as-prepared $Fe_3O_4$ NPs. Figure 3(d) shows that the NPs form an ellipsoid-like aggregate with an irregular surface when exposed to an external static magnetic field in the $x$ direction. The lengths of the obtained aggregates in our experiment are roughly from 15 to 50 μm. The concentration of ellipsoid-like aggregates reveals a quadratic dependence on the concentration of $Fe_3O_4$ NPs under a static magnetic field of 25 Oe, as shown in Fig. 3(e). The concentrations of aggregates were determined using an Olympus BX53 microscope. At the NP concentration of 0.5%, Fig. 3(f) shows that the concentration of ellipsoid-like aggregates is also quadratically dependent on the static magnetic field.

### 3.2 Motion of magnetically controlled $Fe_3O_4$ NP aggregates

To understand the motion behavior of $Fe_3O_4$ aggregates, aggregates with lengths of 15, 25, and 50 μm (denoted as L15, L25, and L50, respectively) under the combined oscillating magnetic field were observed. Figure 4 shows the sequential images of three aggregates of L25 (marked as A, B, and C) subjected to a combined oscillating magnetic field with $H_s$ = 25 Oe, $H_p$ = 8 Oe, and $f$ = 45 Hz. The observation lasts for 7 s to ensure that the motion process can be properly measured. The motion trajectories of the aggregates were observed and recorded with a high-speed camera (Teledyne Dalsa Genie HM640). The video was then divided into separate images

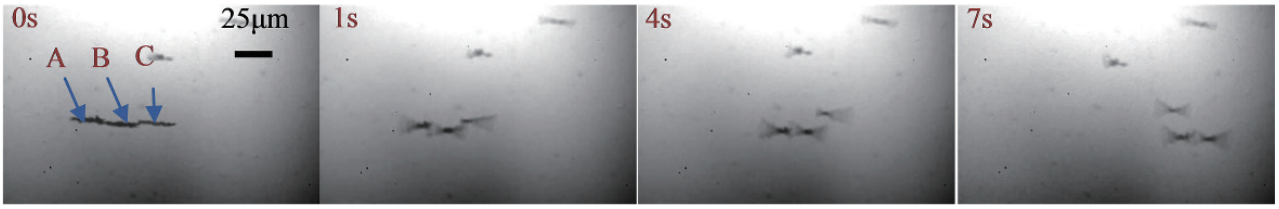


Fig. 4. (Color online) Image sequences show the swaying and translational motion of three ellipsoid-like aggregates (L25) under $H_s$ = 22 Oe, $H_p$ = 8 Oe, and $f$ = 45 Hz.

for the analysis of the instantaneous displacement and velocity of aggregates. Before alternating current is input into the coils, $Fe_3O_4$ NPs aggregate into ellipsoid-like aggregates under a static magnetic field. After the AC current is input into the coils, the aggregates start to oscillate with the orientation of the combined magnetic field. An amplitude of 20.5° of the oscillating magnetic field can be obtained. The observed swaying amplitude of aggregates is almost the same as the amplitude of the combined magnetic field, which means that there exists no phase angle lag. The aggregates are driven towards the magnetic gradient. The translational motion trajectories of five aggregates of L25 in the $x$-axis direction are shown in Fig. 5. The translational velocities of aggregates are varied at different time intervals. This may be caused by the changing fluid resistance induced by the sway motion.

Ureña *et al.*[27] established the theoretical critical frequency for micro-NPs rotating at low Reynolds numbers. The experiments to observe the critical frequency of these ellipsoid-like aggregates in the combined oscillating magnetic field have been performed. The comparable measurements of $Fe_3O_4$ aggregates are carried out from the observations of L15, L25, and L50 and shown in Fig. 6. Figure 6(a) shows the swaying frequencies and amplitudes of L15, L25, and L50 at $H_s$ = 22 Oe and $H_p$ = 8 Oe, varying the magnetic frequencies from 0 to 90 Hz. As shown, the swaying frequencies of L15 and L25 are the same as the magnetic field, and their swaying amplitudes are maintained at 20–22°. The swaying frequency and amplitude of L50 are coincident with those of L15 and L25 when the magnetic field frequency $f$ is lower than 45 Hz. However, they suddenly decrease once the frequency is higher than 45 Hz. This phenomenon is observed when the increased magnetic frequency is beyond the critical frequency of aggregate L50, which agrees with the theoretical result obtained by Ureña *et al.*[27] Figure 6(b) shows that if $H_s$ is fixed at 22 Oe, L15 and L25 maintain the same values as the magnetic field amplitude even when $H_p$ is over 50 Oe. This illustrates that the inertia of these aggregates has little impact on the motion and can be ignored. In addition, the swaying amplitude of L50 gradually becomes lower than the magnetic field amplitude beyond 25 Oe. A bending deformation of aggregate L50 was observed at this stage. This may result in the decline of the amplitude. Figure 6(c) shows the relationship between the swaying amplitude of aggregates and the static magnetic field $H_s$ at $H_p$ = 25 Oe and $f$ = 45 Hz. Accordingly, the swaying amplitudes of L15 and L25 agree with the magnetic field curve very well but the swaying amplitude of L50 is much lower than the magnetic field curve until $H_s$ exceeds 22 Oe. This shows that a stronger static magnetic field is favorable for stabilizing and stiffening the structure. When the static magnetic field is weaker than the alternating magnetic field, the aggregates with larger length are likely deformed by the oscillating field, as has also been found by many researchers.[28–31] The swaying amplitude of aggregate L25 is almost linearly dependent on the relative angle between $H_s$ and $H_v$, as depicted in Fig. 6(d). This angle can

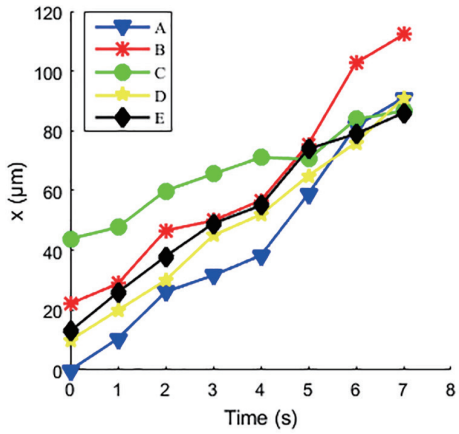


Fig. 5. (Color online) Translational motion trajectories of five aggregates of L25 in the *x*-axis direction for a period of 7 s. The centroid of aggregate "A" at 0 s is set as the original point.

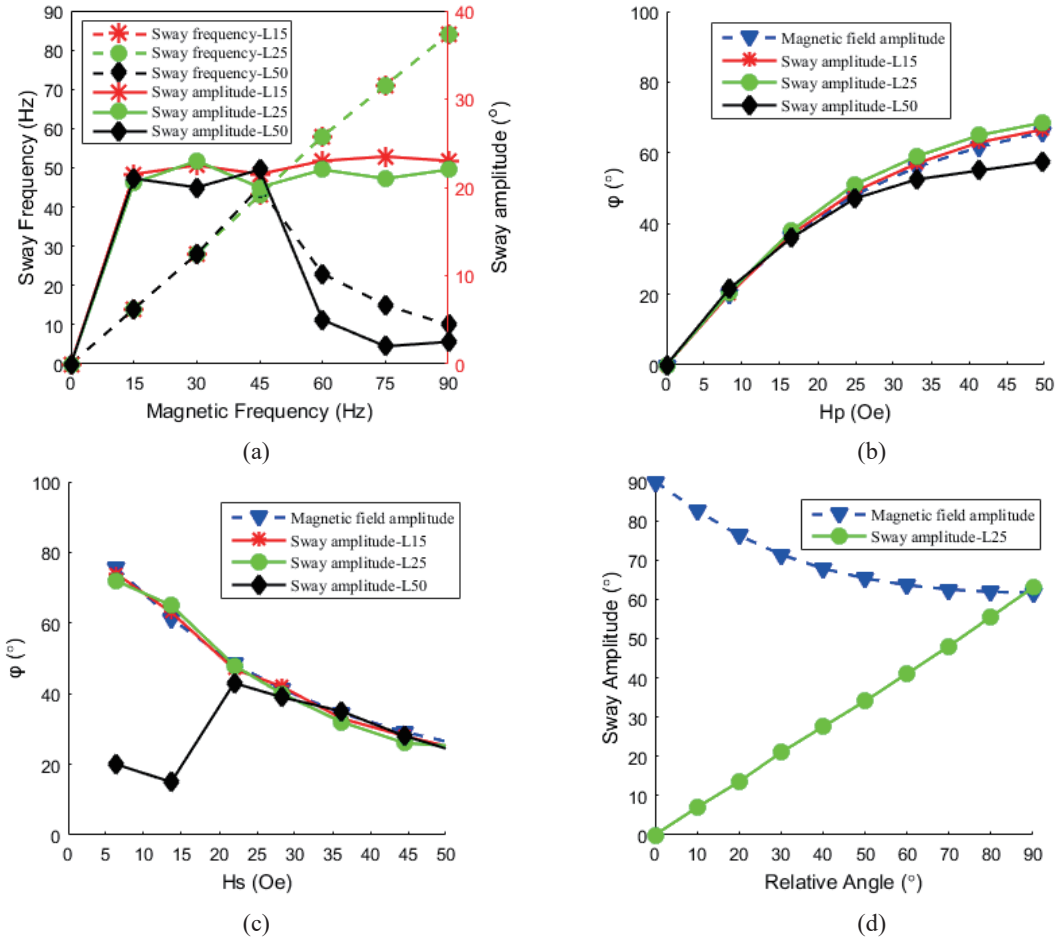


Fig. 6. (Color online) (a) Swaying frequencies and amplitudes of L15, L25, and L50 vary with the magnetic field frequency at $H_s$ = 22 Oe and $H_p$ = 8 Oe. (b) Swaying amplitudes of L15, L25, and L50 vary with $H_p$ at the frequency of 45 Hz and $H_s$ = 22 Oe. (c) Swaying amplitudes of L15, L25, and L50 vary with the static magnetic field $H_s$ at $H_p$ = 25 Oe and $f$ = 45 Hz. (d) Swaying amplitude of L25 varies with the relative angle between $H_s$ and $H_v$.

be adjusted by changing the position of the permanent magnets. The largest swaying amplitude occurs when $H_s$ is orthogonal to $H_v$. The swaying amplitude is significantly different from the magnetic field amplitude, which shows a quadratic relationship with the relative angle until the angle approximately equals 90°. In short, the aggregates can be effectively controlled to sway and translate with the proper configuration of static and dynamic fields.

### 3.3 Softening hard stool with magnetically controlled swaying $Fe_3O_4$ NP aggregates

The analogy of a broom clearing rubbish is usually associated with this motion of $Fe_3O_4$ NP aggregates. These aggregates were used for the softening of hard stool in an artificial intestinal tract. An *in vitro* experiment using a microfluidic capillary with an inner diameter of 0.9 mm was carried out. The permanent magnets and coaxial electromagnetic coils were placed orthogonally to each other. The permanent magnets produced a static magnetic field of $H_s$ = 22 Oe. A current with a frequency of 45 Hz was input into the electromagnetic coils to produce an alternating magnetic field with the amplitude varying from 0 to 33 Oe. Stool from a healthy volunteer was dried into a hard block on an alcohol burner. A small piece of the dried stool and the as-prepared $Fe_3O_4$ NP solution were successively placed into the microfluidic capillary. Then, the ends of the capillary were sealed with plasticine. The sequential images in Fig. 7 show the softening of a large mass of hard stool in the microcapillary. Observations were made using a 10× micro-objective. As shown, with an increase in current amplitude, the hard stool was gradually subjected to perturbation. The center of the stool started to break up when $H_p$ reached 16.5 Oe. With further increase in the current amplitude, the whole stool block started to shake and broke into pieces. These pieces moved up and down, aiding the breaking up of the remaining stool. After about 38 s, the primary stool block had turned into scattered fragments. Here, quantities of aggregates with almost all sizes were used to soften the stool. The results show that various aggregates of any size formed by a magnetic field can be used to break stool.

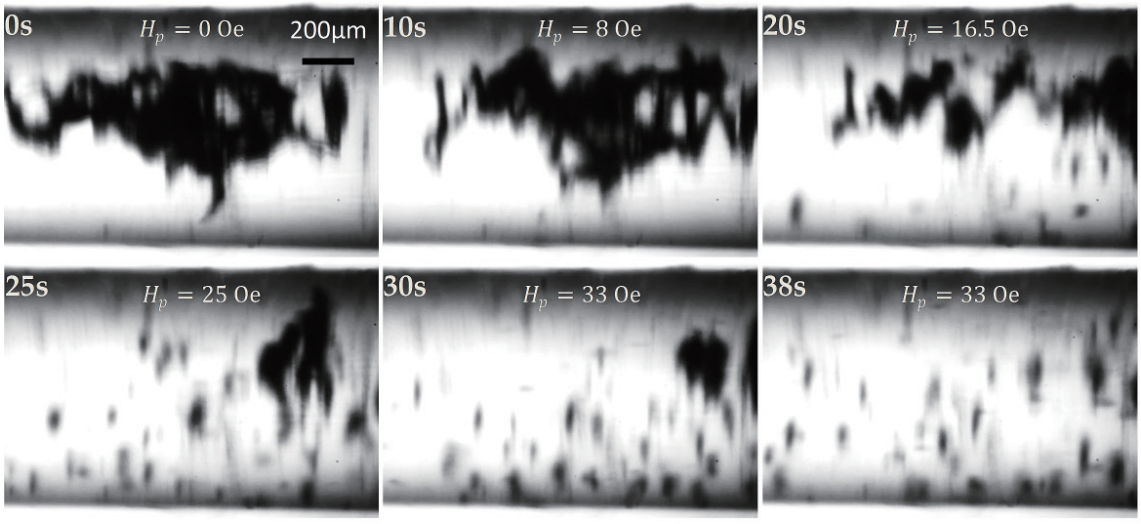


Fig. 7. Image sequences display the softening of hard stool adhesions in microfluidic capillary by magnetically controlled $Fe_3O_4$ aggregates in a microfluidic capillary. A large hard block was broken into pieces within 40 s.

To observe the process more closely, an experiment in a petri dish with a 50× micro-objective was conducted. The sequential images in Fig. 8 show the softening of stool with a single $Fe_3O_4$ NP aggregate. Before the sway-inducing magnetic field was activated, $Fe_3O_4$ NPs formed into an ellipsoid-like aggregate under a static magnetic field of $H_s$ = 22 Oe and was surrounded by messily distributed stool. When a sway-inducing alternating magnetic field with an amplitude of $H_p$ = 33 Oe and a frequency of 45 Hz was activated, the microrod swayed rapidly, breaking up the stool. By adjusting the position of the permanent magnets, the microrod can be pushed forward or pulled back to break the stool in other positions. The aggregate was guided, by varying the magnetic gradient, to come into contact with the stool on the right. The stool was gradually reduced with the movement of the aggregate and cleared at about 24 s. In the whole process, the stool was broken from left to right, which is coincident with the principle described. The aggregate was also damaged by the intense collision. However, the continuous strike results in the formation of an empty space to the right so that the stool pellets can be removed from the clear region of the channel.

## 4. Discussion

Fecal impaction is a gastrointestinal problem in which hard stool obstructs the rectum. The obstruction caused by hard stool has been softened and evacuated to open up a passageway using $Fe_3O_4$ NP aggregates *in vitro*. As is known, $Fe_3O_4$ is also one of the most important spinel-type materials and has gained much attention in the field of bioimaging. Such an operation mechanism is promising for applications in sensing and treating fecal impaction because of the characteristics of being a good MRI contrast agent and high biocompatibility of $Fe_3O_4$ NPs. However, some problems must be solved before they can be applied *in vivo*. The heat generation during hard stool softening may affect the rectum content with possible pain. The control of the temperature rise *in vivo* induced by the magnetic NP motion in an alternating magnetic field is still being studied. However, in our system, the delivered power is not high because of the low frequency of the external magnetic field. Thus, the evacuation of NP residues in the wrinkles of the rectum after the completion of the process should be further studied.

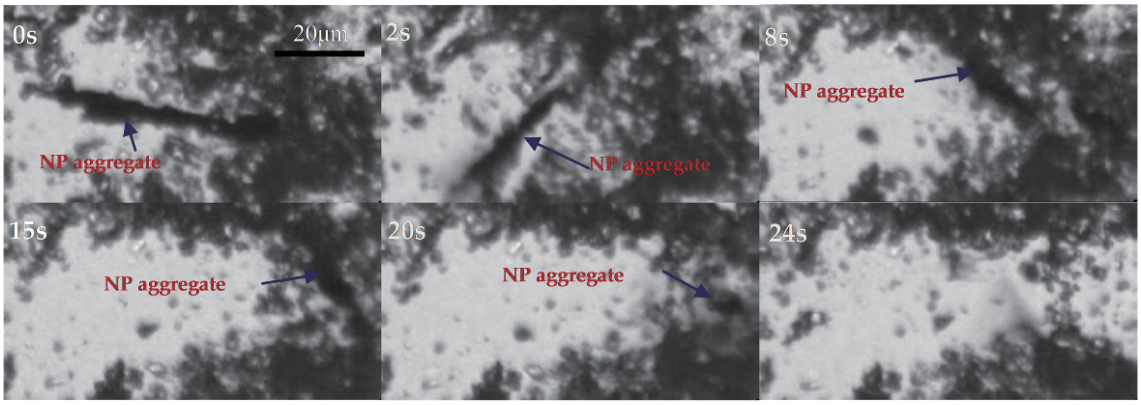


Fig. 8. (Color online) Image sequences display the breaking of stools with swaying $Fe_3O_4$ aggregates observed with a 50× micro-objective.

Certainly, the limitations of our model should be improved for a more realistic *in vivo* environment. Primarily, an isotonic dispersion medium, which is the survival environment of human tissue, should be used in place of the deionized water in the experiment since magnetic NPs behave almost the same in these two media. Moreover, because the characteristics of the dehydrated stool material after heat drying may differ from those of naturally dehydrated stool, the application of NPs to the latter should be investigated next.

However, the stool softening method using $Fe_3O_4$ NPs in a combined oscillating magnetic field has been proposed in this study and verified *in vitro*. Its application in fecal impaction treatment *in vivo* is forecasted in the future. The next step is to explore how to implement early diagnosis and sensing of fecal impaction by combining the motion manipulation of $Fe_3O_4$ NPs and MRI or other bioimaging technologies. Since both motion control and imaging are based on the same materials, such a combination is also expected.

## 5. Conclusions

In the study, we demonstrated the motion of swaying $Fe_3O_4$ NP aggregates using a combined oscillating magnetic field generated by two electromagnetic coils and two permanent magnets. The swaying $Fe_3O_4$ aggregates were employed to soften hard stool in a microfluidic capillary. The whole process was rapid (about 38 s) and required no other artificial intervention than the applied magnetic field. Although only a small block of hard stool was broken in the microfluidic capillary, the softening efficiency is encouraging. Fecal impaction is a common and serious gastrointestinal medical condition involving hard stool obstructing the rectum. Therefore, the detection and softening of hard stool *in vivo* via the noncontact control of biocompatible $Fe_3O_4$ NPs for the treatment of fecal impaction is important and can be expected in the near future.

## Acknowledgments

The authors gratefully acknowledge the support of the State Key Laboratory of Digital Manufacturing Equipment and Technology, Huazhong University of Science and Technology, China and Program for Research Foundation for Advanced Talents of Huaqiao University (Grant No. 16BS504).

## References

1 Z. H. Hussain, D. A. Whitehead, and B. E. Lacy: Curr. Gastroenterol. Rep. **16** (2014) 404.
2 F. Araghizadeh: Clin. Colon. Rect. Surg. **18** (2005) 116.
3 B. S. Falcón, M. B. López, B. M. Muñoz, A. Á. Sánchez, and E. Rey: BMC Geriatrics **16** (2016) 4.
4 C. E. Chumpitazi, E. B. Henkel, K. L. Valdez, and B. P. Chumpitazi: J. Pediatr. Gastroenterol. Nutr. **63** (2016) 15.
5 R. Hernu, M. Cour, F. Wallet, and L. Wallet: Am. J. Emerg. Med. **52** (2017) 13.
6 S. Guiyun, S. Y. Chang, W. K. Chan, Y. K. Jae, Y. J. Tae, H. K. Kyung, S. Y. Song, S. Y. Yong, L. Seok-Byung, and C. K. Jin: J. Korean Soc. Coloproctol. **27** (2011) 180.
7 K. Lehto, M. Hyöty, P. Collin, H. Huhtala, and P. Aitola: Int. J. Colorectal. Dis. **28** (2013) 653.
8 R. P. Friedrich, J. Zaloga, E. Schreiber, I. Y. Tóth, E. Tombácz, S. Lyer, and C. Alexiou: Nanoscale Res. Lett. **11** (2016) 1.
9 X. Li, J. Wei, E. K. Aifantis, Y. Fan, Q. Feng, F. Z. Cui, and F. Watari: J. Biomed. Mater. Res. A **104** (2016) 1285.

10 M. Shaalan, M. Saleh, M. El-Mahdy, and M. El-Mahdy: Nanomed-Nanotechnol. **12** (2016) 701.
11 D. L. Fan, F. Q. Zhu, R. C. Cammarata, and C. L. Chien: Phys. Rev. Lett. **94** (2005) 247208.
12 W. Wang, L. A. Catro, and H. Hoyos: ACS Nano **6** (2012) 6122.
13 R. S. M. Rikken, R. J. M. Nolte, J. C. M. Hest, D. A. Wilson, and P. C. M. Christianen: Soft Matter **10** (2014) 1295.
14 L. Zhang, T. Petit, K. Peyer, and B. J. Nelson: Nanomed-Nanotechnol. **8** (2012) 1074.
15 Y. Zhou and S. Metin: Lab Chip **14** (2014) 2177.
16 J. L. F. Gabayno, D. W. Liu, M. Chang, and Y. H. Lin: Nanoscale **7** (2015) 3947.
17 M. Chang, Y. H. Lin, J. L. Gabayno, Q. Li, and X. Liu: Bioengineered **8** (2017) 29.
18 A. Chanu and S. Martel: Med. Biol. Soc. **29** (2007) 6584.
19 K. B. Yesin, K. Vollmers, and B. J. Nelson: Int. J. Robot. Res. **25** (2006) 527.
20 H. Choi, J. Choi, G. Jang, J. Park, and S. Park: Smart Mater. Struct. **18** (2009) 055007.
21 J. Einarsson, B. M. Mihiretie, A. Laas, S. Ankardal, and J. R. Angilella: Phys. Fluids **28** (2016) 013302.
22 J. J. Abbott, O. Ergeneman, M. P. Kummer, A. M. Hirt, and B. J. Nelson: IEEE T. Robot. **23** (2007) 1247.
23 T. Qiu, T. C. Lee, A. G. Mark, K. I. Morozov, R. Münster, O. Mierka, S. Turek, A. M. Leshansky, and P. Fisher: Nat. Commun. **5** (2014) 5119.
24 K. Chatterjee, S. Sarkar, K. J. Rao, and S. Paria: Adv. Colloid. Interfac. **209** (2014) 8.
25 E. J. Furlani and E. P. Furlani: J. Magn. Magn. Mater. **312** (2007) 187.
26 S. Sharma, V. K. Katiyar, and U. Singh: J. Magn. Magn. Mater. **379** (2015) 102.
27 E. B. Ureña, Y. Mei, E. Coric, E. Coric, D. Makarov, M. Albrecht, and O. G. Schmidt: J. Phys. D: Appl. Phys. **42** (2009) 055001.
28 Y. Gao, A. van Reenen, M. A. Hulsen, A. M. de Jong, M. W. J. Prins, and J. M. J. den Toonder: Microfluid. Nanofluid. **16** (2014) 265.
29 C. Velez, I. Torres-Díaz, L. Maldonado-Camargo, C. Rinaldi, and D. P. Arnold: ACS Nano **9** (2015) 10165.
30 T. G. Kang, M. A. Hulsen, P. D. Anderson, J. M. Toonder, and H. E. Meijer: Phys. Rev. E **76** (2007) 066303.
31 Y. H. Li, E. Bansal, and C. Y. Chen: Magnetohydrodynamics **50** (2014) 1.

## About the Authors

**Qian Li** received his B.S. degree from Wuhan University of Science and Technology, China, in 2012 and his M.S. degree from Huazhong University of Science and Technology, China, in 2015. He is now a Ph.D. candidate in Huazhong University of Science and Technology. His research interests include nanomaterials and bioengineering.

**Xiaojun Liu** received his B.S. degree from Harbin Institute of Technology, China, in 1990, his M.S. degree from Huazhong University of Science and Technology, China, in 1996, and his Ph.D. degree from The Hong Kong University of Science and Technology, China, in 2003. He is currently a full professor in the School of Mechanical Science and Engineering at Huazhong University of Science and Technology, China. At present he is a deputy director of the research center for international standards of manufacturing technology, Ministry of Education and a member of a specialized committee of the China Metrology and Measurement Society. His research interests are in optical precision measuring techniques and instruments, surface measurement and analysis, precision engineering, and bioengineering.

**Ming Chang** received his B.S. degree from National Central University, Taiwan, in 1976 and his M.S. and Ph.D. degrees from National Taiwan University, Taiwan, in 1980 and 1986, respectively. Since 1994, he has been a full professor in the Department of Mechanical Engineering at Chung Yuan Christian University, Taiwan. At present he is also a director of the Chinese Metrology Society and vice president of the Taiwan Automatic Optical Inspection Equipment Association. His research interests include automated optical inspection, precision metrology, and bioengineering.

**Wei Hsiu Lin** received his B.S. degree from I-Shou University, Taiwan, in 2009, and his M.S. degree from Chung Yuan Christian University, Taiwan, in 2011. He is now is a Ph.D. candidate in Chung Yuan Christian University, Taiwan. His research interests include automated optical inspection, application of nanomaterials, and system integration.

**Zhen Lu** received her B.S. degree from Henan Normal University, China, in 2012 and her M.S. degree from Huazhong University of Science and Technology, China, in 2015. She is now an instructor at Shanghai University of Electric Power, China. Her research interests include nanomaterials and bioengineering.